

# Development of Variable-View-Factor and Deployable Two-Phase Radiator

Jeff Diebold<sup>1</sup>, Calin Tarau<sup>2</sup>, Andrew Lutz<sup>3</sup> and Srujan Rokkam<sup>4</sup>  
*Advanced Cooling Technologies, Inc., Lancaster, PA, 17601*

Radiators for manned spacecraft, satellites, planetary rovers and unmanned spacecraft are typically sized for the highest power at the hottest sink conditions, so they are oversized and prone to freezing at low sink temperatures. In order to address the need for light-weight and efficient radiators capable of a significant heat rejection turndown ratio, Advanced Cooling Technologies, Inc. (ACT) has developed a novel vapor-pressure-driven variable-view-factor and deployable radiator that passively operates with variable geometry (i.e., view factor). The device utilizes two-phase heat transfer and novel geometric features that passively (and reversibly) adjust the view factor in response to internal pressure in the radiator. This paper extends previous 2D structural modeling to three dimensions. A set of important geometric variables are identified and their influence on the view factor is parametrically investigated. In addition, a thermal model of the variable-view-factor two-phase radiator is introduced and used to demonstrate the thermal control capabilities of the concept.

## Nomenclature

$A$	= area
$\varepsilon$	= emissivity
$\eta$	= radiator efficiency
$h_c$	= heat transfer coefficient of condensation
$H$	= height of radiator
$k$	= thermal conductivity
$Q$	= heat load
$R$	= bend radius
$\sigma$	= Stefan-Boltzmann constant
$t$	= wall thickness
$T_{rad}$	= radiator temperature
$T_s$	= heat sink temperature
$T_v$	= vapor temperature
$\theta$	= profile angle
$V_f$	= view factor
$VVFTPR$	= variable-view-factor two-phase radiator
$Z$	= depth of radiator

## I. Introduction

Radiators for spacecraft and satellites are sized for the highest power at the hottest sink conditions, and are therefore oversized most of the time and prone to freezing when the heat sink temperature and heat loads are low. There is a need to develop light-weight and efficient radiators for future spacecraft and satellites which offers the capability of significant heat rejection turndown.<sup>1,2</sup> The 2015 NASA Thermal Technology Roadmap says that NASA is looking for Variable Geometry Radiators,<sup>3</sup> “The development goal is to provide radiators with a 6:1 (with a stretch goal of 12:1)

<sup>1</sup> R&D Engineer, R&D, 1046 New Holland Ave.

<sup>2</sup> Principal Engineer, R&D, 1046 New Holland Ave.

<sup>3</sup> R&D Engineer, R&D, 1046 New Holland Ave.

<sup>4</sup> Lead Engineer, R&D, 1046 New Holland Ave.

heat rejection turndown capability.” ACT has developed a passive, variable-geometry radiator that has the possibility of turndown ratios greater than 40:1.<sup>4</sup>

For spacecraft and planetary thermal control applications, it is essential to maintain survivable operational temperatures for onboard devices and minimize temperature fluctuation when the heat load and/or the environmental temperature changes drastically. Under a Small Business Innovation Research (SBIR) project funded by NASA Marshall Space Flight Center, Advanced Cooling Technologies, Inc. (ACT) developed a novel *vapor-pressure-driven variable-view-factor and deployable radiator* that passively operates with variable geometry (i.e., view factor) and offers high heat rejection turndown ratio. The advantages of the variable-view-factor radiator over a conventional flat panel radiator include:

- *Passive temperature control*: Variable thermal resistance minimizes temperature swings despite changes in operating or environmental conditions. This feature will maintain the electronics above the minimum operating temperature even during times of low heat loads and low heat sink temperatures.
- *Survival*: In the fully closed position, heat rejection from the radiator is minimized resulting in a reduction in the required survival heater power.
- *Deployable*: During launch the radiator is in a compact configuration allowing for simplified storage.

Previous work by Lutz et al.<sup>4</sup> included experimental prototype testing and 2D parametric structural studies. The focus of the current paper is on introducing updates to the variable-view-factor radiator concept, extending the structural modeling to three dimensions and introducing a thermal model of the radiator. The structural and thermal models are linked through a calculation of the view factor of the deformed surface.

## II. Variable View Factor Concept

The basic concept of the variable-view-factor two-phase radiator (VVFTPR) is illustrated in Figure 1 alongside images of the Phase I prototype in operation.<sup>4</sup> The flexible actuator section of the VVFTPR consists of a hollow curved panel that is filled with a two-phase working fluid and sealed. An increase in fluid temperature results in a higher vapor pressure within the hollow curved panel causing the radiator to open. This opening increases the effective view factor to space of the radiator allowing more heat to be dissipated while minimizing the rise in vapor temperature.

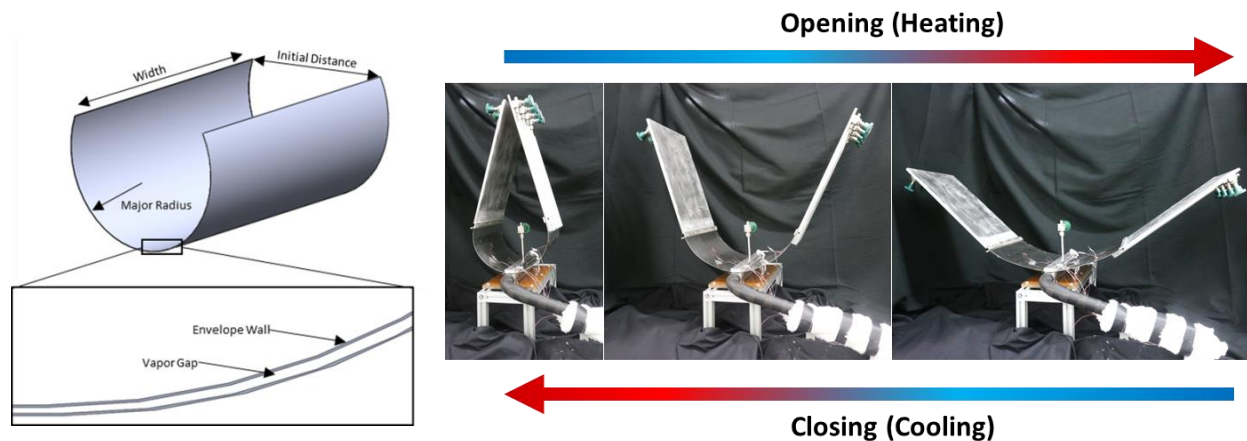


**Figure 1. Schematic of VVFTPR flexible section and images of the Phase I prototype.**

The VVFTPR developed at ACT by Lutz et al.<sup>4</sup> demonstrated several key features:

- *High Heat Rejection Turndown Ratio*: Modeling and experimental work for the Phase I prototype, shown in Figure 1, demonstrated a heat rejection turndown ratio of 37:1.
- *Passive Thermal Control*: The VVFTPR uses vapor pressure to passively change the shape of the radiator with no need for external power, equipment, or control mechanism.
- *Fast Response*: Experimental results demonstrated that the variable-view-factor radiator morphing behavior was mainly temperature dependent. The time scale of morphing due to vapor pressure changes was negligible relative to temperature changes of the wall material due to both conduction and thermal inertia.
- *Reversible and highly durable*: The radiator was designed to operate within the elastic domain of the material and was therefore reversible.

- *High radiator efficiency:* Standard heat pipe radiators rely on fins to spread the heat away from the pipe. This results in a non-uniform temperature distribution and reduces the radiator efficiency. The entire surface of the VVFTPR will be nearly isothermal resulting in an improved efficiency from 0.85 to near 1.0.

While the Phase I prototype proved very successful, several updates to the design concept are being explored. Figure 2 highlights the main features of the previous and updated design concepts. The flexible panel of the Phase I prototype was constructed from stainless steel sheets welded along the seam to form a single vapor space. Spot welds were placed periodically across the flexible section in order to prevent ballooning of the envelope. Heat was then spread to a separate flat panel via heat pipes adhered to the back of the panels as shown in Figure 2a. ACT is currently investigating the following improvements to the design:

- *Envelope material:* Different envelope materials will be explored. Stainless steel offers high yield stress while aluminum alloys offer reduced Young’s modulus and weight reduction.
- *Modular Channels:* The vapor space will be divided into several modular channels along the span of the radiator as shown in Figure 2b. This will improve the reliability of the radiator because a single leak, potentially caused by micrometeorite damage, will not result in the loss of all of the working fluid.
- *Continuous Vapor Space:* The modular channels will be constructed so that the flexible panel and the straight panel contain a single continuous vapor space. This will reduce thermal resistance and result in a high efficiency radiator due to the nearly isothermal surface.
- *Structural Support:* Ribs can be applied to the surface of the straight panel in order to contain the high internal pressure with a minimum wall thickness.

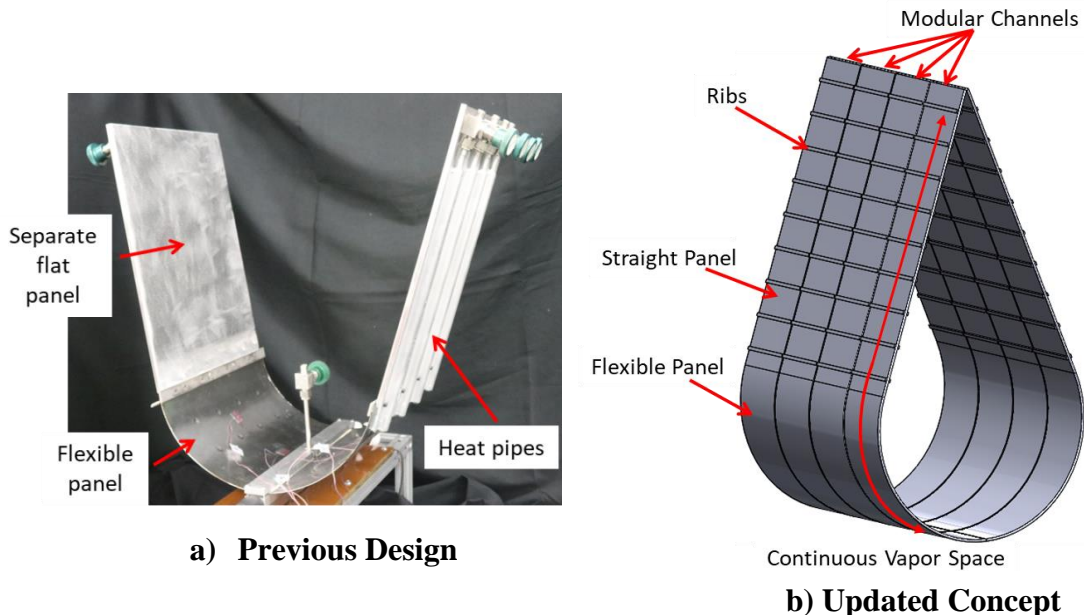


**Figure 2. Overview of previous design concept and the updated design concept for the variable-view factor two-phase radiator.**

### III. Theoretical Analysis

#### A. 3D Geometry and Structural Modeling

Previous work done by ACT included a parametric study of VVFTPR geometry using 2D structural simulations.<sup>4,5</sup> The parametric study investigated the effects of various features including the bend radius of the flexible panel, envelope wall thickness, and vapor space gap. This section discusses 3D structural modeling of the VVFTPR currently underway at ACT. The purpose of the 3D structural simulations is to continue a parametric investigation of the geometry and to help in the development of a thermal model of the VVFTPR discussed later in this paper. All structural simulations discussed in this paper were carried out using Abaqus SIMULIA.

Figure 3 shows the 3D model used for simulations as well as the variables used to define the profile shape of the VVFTPR. Simulations were conducted for a 1/4 model of a single modular channel with symmetry boundary conditions

applied along two edges as shown in Figure 3. When the VVFTPR is in the fully-closed position the profile creates a tear-drop shape defined by the parameters  $\theta$  and  $R$ . For a given application of the VVFTPR, the design will be constrained by the maximum allowable width  $2R$ , height  $H$  and depth  $Z$ . The depth is controlled by the width of the modular channels and the number of channels used. The total effective surface area available for heat transfer is a function of  $R$ ,  $\theta$  and  $Z$ , as well as the view factor of the radiator at the maximum design vapor pressure which is limited by the maximum allowable temperature. A special case of the profile shown in Figure 3 occurs when  $\theta = 90^\circ$ . In this case, the profile becomes a circle which represents the most compact cross-sectional profile of the VVFTPR.

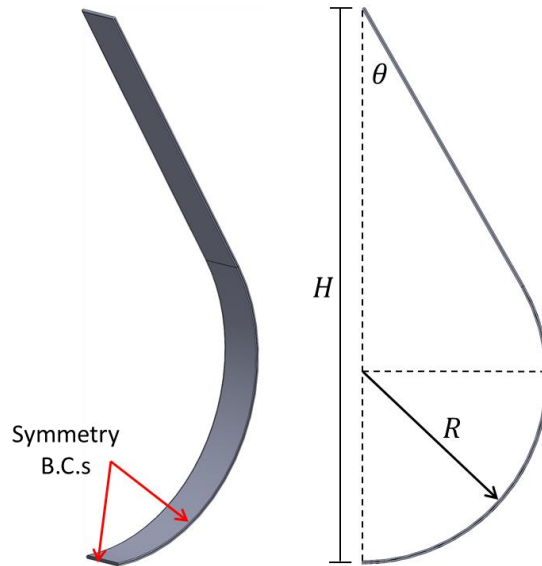


**Figure 3. 3D Model for simulations and relevant geometric variables.**

Figure 4 shows the geometry of the modular channel used in the 3D structural simulations. The relevant variables include the wall thickness, the channel width and the height of the vapor space gap. Due to uncertainty in the geometry of the modular channels at the edges due to the welding process the simulations were performed assuming a circular profile of the edge as shown in Figure 4.

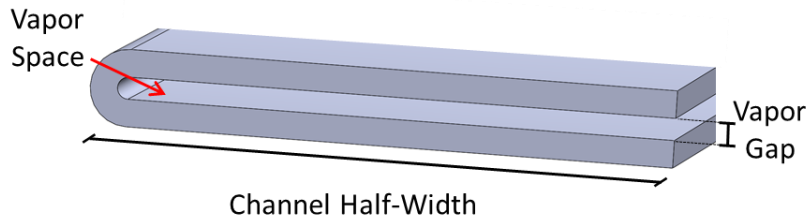


**Figure 4. Geometry of the modular channel used for 3D simulations.**

The effect of the vapor pressure on the 3D model was simulated by applying a uniform pressure to all internal surfaces of the 3D model. Due to the expected large displacements, the simulations carried out in Abaqus SIMULIA were set to nonlinear mode. This setting accounts for geometric nonlinearity due to large deformation of the structure. The material was assumed to remain in the linear region and therefore nonlinear behavior due to plastic deformation was not modeled. All simulations were performed assuming the envelope material was aluminum with a modulus of elasticity of  $10 \times 10^6$  psi.

## B. View Factor Calculation

The effective surface area available for radiative heat transfer will depend on both the physical surface area of the radiator and the view factor obtained at a given pressure. The view factor between two surfaces  $i$  and  $j$  is defined as the proportion of radiation leaving surface  $i$  and striking surface  $j$  and can be calculated by Eq. (1).

$$V_{f,ij} = \frac{1}{A_i} \iint \frac{\cos(\phi_i) \cos(\phi_j)}{\pi L^2} dA_i dA_j \quad (1)$$

Where  $\phi$  represents the angle between the lines connecting the differential elements  $dA_i$  and  $dA_j$  and their respective surface normals.  $L$  represents the distance between the differential elements.

For a given design, the VVFTPR can be divided into four surfaces forming an enclosure shown in Figure 5. The fully closed profile shown in Figure 5 corresponds to the case of  $\theta = 90^\circ$ . Surface 1 represents the radiating surface of the VVFTPR, Surface 2 represents the plane formed at the exit of the radiator and Surfaces 3 and 4 represent the end caps.

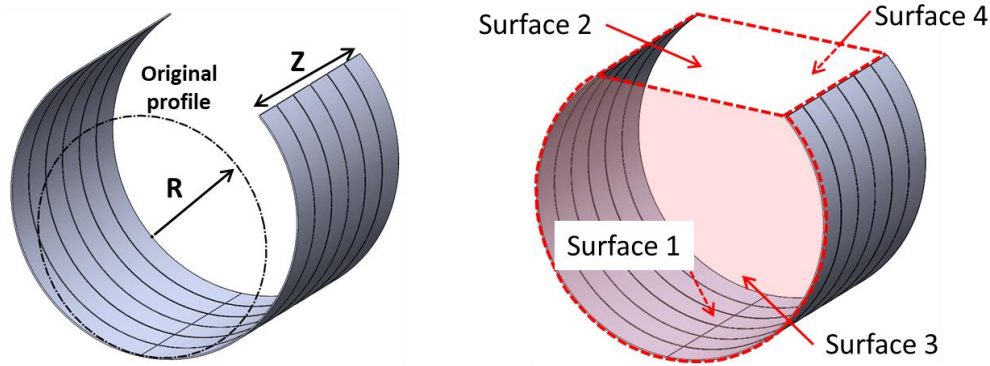


**Figure 5 Surfaces used for view factor calculation.**

For the purposes of this paper, it will be assumed that no heat radiates through the end caps and the view factor relevant to heat transfer is  $V_{f,12}$ . For the fully closed condition, surfaces 3 and 4 could represent fixed surfaces. As the radiator deforms it would not be possible to fully block surfaces 3 and 4, nor would it be desirable as this would reduce the view factor. For this paper, considering only  $V_{f,12}$  represents a conservative estimate of the maximum view factor while still allowing the minimum view factor to go to zero. For a given design and internal vapor pressure a 3D structural simulation was used to determine the deformed profile. This profile along with a value of  $Z$  was then used in Eq. (1) to calculate  $V_{f,12}$ . The integration of Eq. (1) was carried out numerically.

## C. Thermal Modeling

In an actual application heat would flow from a source, such as electronics, into the saturated two-phase working fluid within the VVFTPR. The excess heat would cause the temperature and therefore pressure of the vapor to increase resulting in an opening of the radiator and an increase in view factor until the radiating heat transfer, given by Eq. (2), balances the heat input from the source  $Q$ .

$$Q = \sigma \epsilon \eta V_{f,12} A (T_{rad}^4 - T_s^4) \quad (2)$$

In Eq. (2)  $\sigma$ ,  $\epsilon$  and  $\eta$  represent the Stefan Boltzmann constant, the emissivity of the surface and the efficiency of the radiating surface, respectively. Due to the two-phase heat transfer within the vapor space of the VVFTPR the surface of the radiator is assumed to be isothermal resulting in an efficiency of 1.0.  $T_{rad}$  and  $T_s$  represent the temperature of the radiating surface and the sink, respectively.

The purpose of the variable-view-factor feature is to passively maintain the temperature of the heat source within a narrow band while the sink temperature  $T_s$  and power input  $Q$  vary over a wide range. The temperature drop between the source and the vapor will depend on the exact layout of the source and spacecraft and therefore will be application dependent. For the purpose of modeling and designing a VVFTPR it will be sufficient to investigate the change in

vapor temperature  $T_v$  as the sink temperature  $T_s$  and power input  $Q$  change. This can be done through the use of a thermal resistance model between vapor temperature and sink. This model accounts for resistance due condensation on the inner surface of the VVFTPR, conduction through the envelope and radiation from the radiator surface. Radiation from the back surface of the VVFTPR is assumed to be negligible. The heat transfer from vapor to sink can be expressed using Eq. (3).

$$Q = \frac{T_v - T_s}{\frac{t}{kA} + \frac{1}{h_c A} + \frac{1}{\sigma \epsilon \eta V_{f,12} A (T_{rad}^2 + T_s^2) (T_{rad} + T_s)}} \quad (3)$$

In Eq. (3),  $t$ ,  $k$  and  $h_c$  represent the envelope wall thickness, thermal conductivity of the envelope and the heat transfer coefficient of condensation, respectively. For the results presented here the envelope is made from aluminum with a thermal conductivity of  $150 \text{ Wm}^{-1}\text{K}^{-1}$  and the heat transfer coefficient of condensation was assumed to be  $7500 \text{ Wm}^{-2}\text{K}^{-1}$ .

For a given  $T_s$  and  $Q$ , Eqs. (2) and (3) represent a system with three unknowns:  $T_v$ ,  $T_{rad}$  and  $V_{f,12}$ . The thermal model of Eqs. (2) and (3) was coupled with the structural response of the VVFTPR through the use of the 3D structural simulations discussed above. Simulations were performed for several pressures corresponding to the relevant vapor temperature range in order to computationally generate data relating the view factor to the vapor temperature.

$$V_{f,12} = f(P_v(T_v)) \quad (4)$$

Equation (4) was represented by interpolating over the results of a series of structural simulations. Equations (2), (3) and (4) represent a closed system of nonlinear equations that can be used to determine  $T_v$  as a function of  $T_s$  and  $Q$ . These equations were numerically solved with the use of Mathcad 15.

## IV. Simulation and Modeling Results

### A. Effect of Channel Geometry

This section serves as an extension of the parametric study conducted by Lutz et al.<sup>4</sup> to 3D geometry. The results presented here demonstrate the effects of the channel geometry variables (channel width, vapor space gap and wall thickness) on the view factor  $V_{f,12}$  for a radiator profile with  $R = 4.0$  in. (10.16 cm) and  $\theta = 90^\circ$ . Recall that  $\theta = 90^\circ$  results in a circular profile as opposed to a tear-drop shape when fully closed. In order to calculate the view factor, a value of  $Z$  is necessary. For the results presented in this section a value of  $Z = 12.0$  in. (30.5 cm) was selected. A different value of  $Z$  would change the magnitude of  $V_{f,12}$  but not the general trends.

Figure 6 shows the variation of  $V_{f,12}$  as the channel width was increased from 2.0 in. (5.08 cm) to 3.0 in. (7.62 cm) for two values of the internal pressure. The wall thickness and vapor space gap were 0.025 in. (0.635 mm) and 0.02 in. (0.508 mm), respectively. Increasing the channel width for a given internal vapor pressure resulted in an increase in the view factor. The effect of channel width was minor at low pressures but increased nonlinearly as the pressure was increased. The effect of channel width on opening sensitivity of the VVFTPR was due to an increase in surface area and a reduced influence of the edges

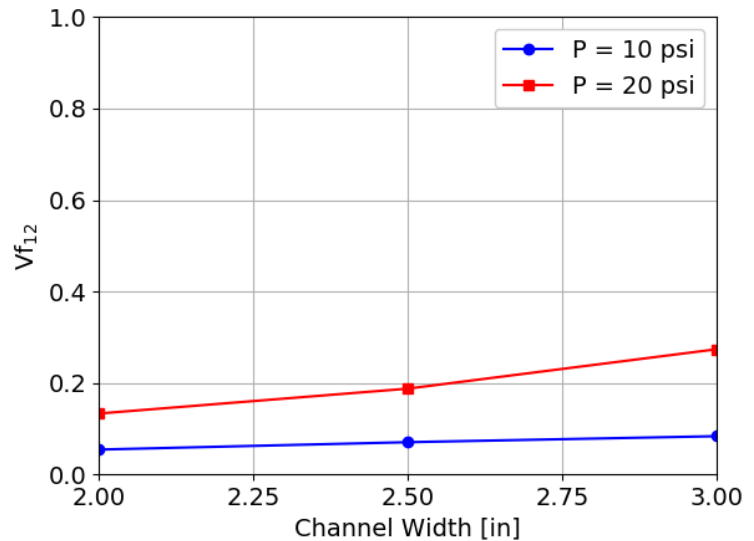
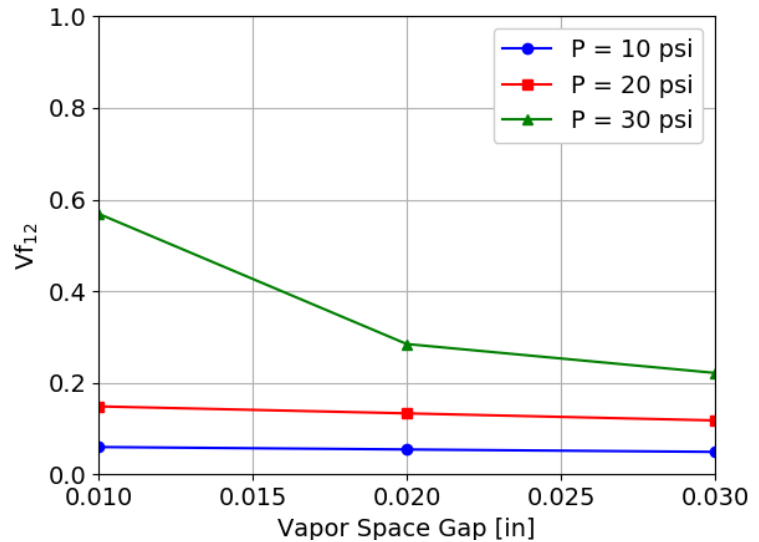


**Figure 6. Effect of channel width on the view factor  $V_{f,12}$ .  $R = 4.0$  in.,  $\theta = 90^\circ$ , wall thickness = 0.025 in., vapor space gap = 0.02 in.,  $Z = 12.0$  in.**

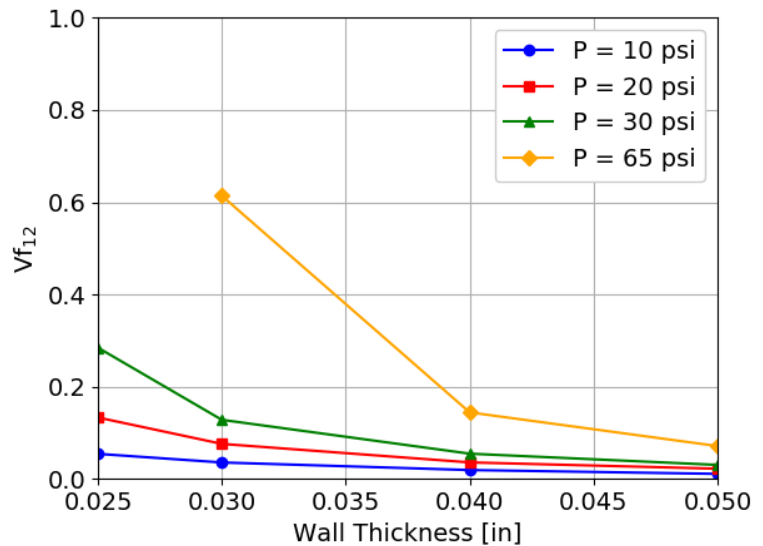
of the channel for the 3D geometry. While increasing the channel width resulted in a higher view factor there are two tradeoffs that must be considered. First, wider channels will result in higher stresses along the edge of the channels. Second, for a given value of  $Z$ , which may be limited by space constraints, increasing the channel width will result in fewer channels and the potential for reduced reliability of the VVFTPR.

Figure 7 shows the variation of  $V_{f,12}$  as the vapor space gap was increased from 0.01 in. (0.254 mm) to 0.03 in. (0.762 mm) for internal pressures of 10, 20 and 30 psi (68.9, 137.8 and 206.7 kPa). The wall thickness and channel width were 0.025 in. (0.635 mm) and 2.0 in. (5.08 cm), respectively. Increasing the vapor space gap resulted in a decrease in the view factor and the effect was nonlinearly dependent on the pressure. This trend is opposite to that observed by Rokkam et al.<sup>5</sup> For the 2D parametric studies it was observed that increasing the vapor space gap resulted in an increase in view factor. The reason for this discrepancy is that increasing the vapor space gap results in two competing effects. First, it increases the surface area of the outer surface of the envelope relative to the inner surface resulting in larger opening for a given pressure. Second, a larger vapor space gap results in increased resistance to bending of the channel. In 2D only the first effect is present but in 3D, the results of Figure 7 indicate that the second effect dominates. While a smaller vapor space gap may be beneficial structurally it will negatively affect the vapor flow within the channel. A smaller area for vapor flow will result in increased pressure drop of the flowing vapor and can limit the maximum power transported through the channel. It is also important to note that the vapor space gap will change with pressure as the radiator surface deforms.

Figure 8 shows the variation of  $V_{f,12}$  as the wall thickness was increased from 0.025 in. (0.635 mm) to 0.05 in. (1.27 mm) for internal pressures of 10, 20, 30 and 65 psi (68.9, 137.8, 206.7 and 447.9 kPa). The channel width and vapor space gap were 2.0 in. (5.08 cm) and 0.02 in. (0.508 mm), respectively. Note that the case for a wall thickness of 0.025 in. (0.635 mm) was not simulated at 65 psi (447.9 kPa) because it would be well outside of the elastic range of the material. As expected, increasing the wall thickness resulted in a significant decrease in the view factor for a given internal pressure. The effect of increasing the wall thickness was heavily dependent on the internal pressure. The wall thickness will primarily be dictated by the need to contain the internal pressure and will be dependent on the operating temperature range and working fluid selection. In addition to reducing the stresses in the envelope a thicker wall will also offer more resistance to damage from micrometeorites and orbital debris; however,



**Figure 7.** Effect of vapor space gap on the view factor  $V_{f,12}$ .  $R = 4.0$  in.,  $\theta = 90^\circ$ , wall thickness = 0.025 in., channel width = 2.0 in.,  $Z = 12.0$  in.



**Figure 8.** Effect of wall thickness on the view factor  $V_{f,12}$ .  $R = 4.0$  in.,  $\theta = 90^\circ$ , vapor space gap = 0.02 in., channel width = 2.0 in.,  $Z = 12.0$  in.

given the sensitivity of the view factor to the wall thickness, designs that minimize this thickness will be optimal. The increased stresses in the thinner walls can be partially compensated by reducing the channel width.

### B. Effect of Profile Shape

While the previous section investigated the effects of the channel geometry this section explores the effects of the profile shape of the VVFTPR on the view factor. As discussed in Section III the profile shape of the VVFTPR is determined by the bend radius  $R$  and the angle  $\theta$  (the height  $H$  results from these two parameters). From a design perspective the relevant constraints will be the width  $2R$ , the height  $H$  and depth  $Z$ . For a given vapor pressure, the depth  $Z$  will not influence the opening but it will affect the calculated view factor. The four profiles presented in this section are summarized in Table 1, refer back to Figure 3 for a description of the relevant variables. The profiles corresponding to Table 1 are shown in Figure 9. Two circular profiles ( $\theta = 90^\circ$ ) of bend radii of 4.0 in. (10.16 cm) and 6.0 in. (15.24 cm) were simulated. The remaining two cases ( $\theta = 19.5^\circ$  and  $\theta = 11.5^\circ$ ) were selected to double and triple the height  $H$  of the 4.0 in. (10.16 cm) radius circular profile. The profiles simulated in this section all used the same channel geometry with a wall thickness of 0.025 in. (0.635 mm), channel width of 2.0 in. (5.08 cm) and vapor gap height of 0.02 in. (0.508 mm) and a differential pressure range of 0 to 35 psi (241.3 kPa).

**Table 1. Geometry of the four profiles.**

$R$ (in.)	$H$ (in.)	$\theta$ (deg.)
6.0	12.0	90.0
4.0	8.0	90.0
4.0	16.0	19.5
4.0	24.0	11.5

Figure 9 shows the effect of internal pressure on the shape of the VVFTPR for the profiles listed in Table 1. It can be seen that the response to pressure was nonlinear. For the case of  $R = 6.0$  in. (15.24 cm) the opening sensitivity was initially low then increased from  $P = 15$  to 25 psi (103.4 to 172.3 kPa) and then decreased again. When  $R = 4.0$  in. (10.16 cm) the opening sensitivity increased monotonically with pressure. For the tear-drop shaped profiles the opening angle appears to increase slightly as  $\theta$  is reduced ( $H$  increased) and there is a significant increase in the available surface area resulting from extending the straight section of the radiator.

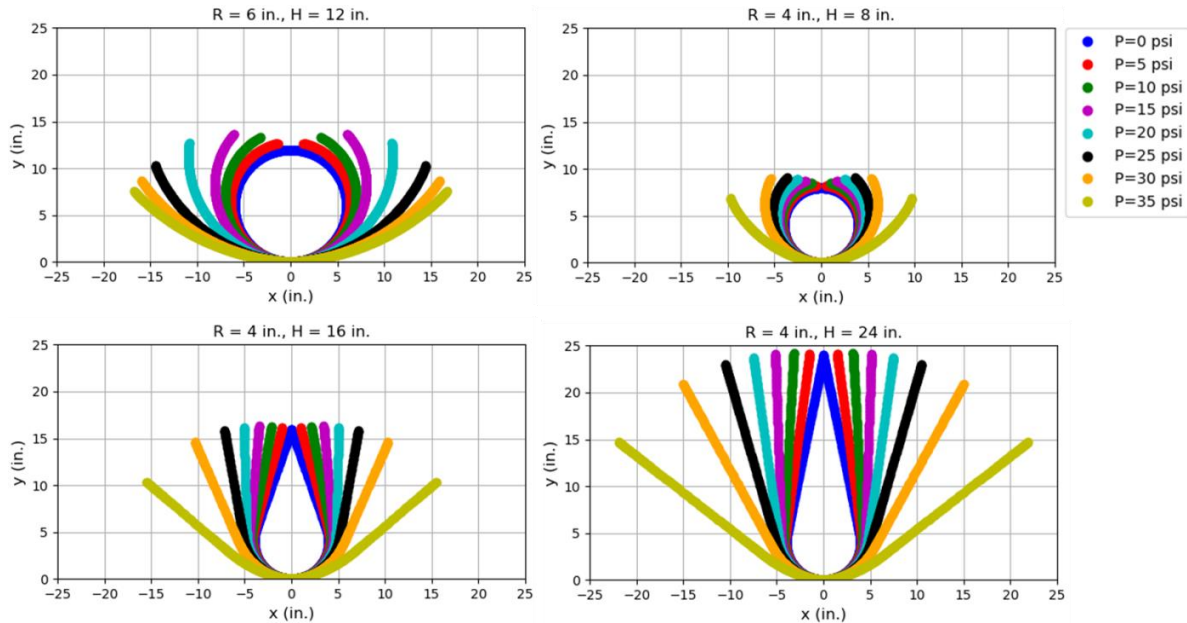


**Figure 9. Effect of pressure on the shape of the VVFTPR for several profile shapes. Wall thickness = 0.025 in., channel width = 2.0 in. and vapor space gap = 0.02 in.**

These trends are more obvious in Figure 10 which shows the effective area (the product of area and view factor)  $AV_{f,12}$  of the VVFTPR profiles as a function of pressure for several values of radiator depth  $Z$ . The effective area is a relevant metric with which to compare different radiator shapes as this parameter controls the heat transfer. As

expected, increasing  $Z$  increased the effective area due to both an increase in view factor and the larger surface area. While  $Z$  does not influence the deformed shape of the VVFTPR the view factor is influenced because of a reduced effect of the end caps.

For the case of a circular profile and a given value of  $Z$ , the larger bend radius resulted in a higher effective area due to both the larger circumference and the increased opening sensitivity for pressures below approximately 25 psi (172.3 kPa). The 6.0 in. (15.24 cm) bend radius exhibited an inflection point in the curve of effective area vs. pressure that was not observed for the 4.0 in. (10.16 cm) radius case. Above approximately 25 psi (172.3 kPa) the 6.0 in. (15.24 cm) radius profile exhibited decreased sensitivity to the pressure, while the sensitivity of the 4.0 in. (10.16 cm) radius case continued to increase as the pressure rose. This trend was also observed for the tear-drop profiles with a 4.0 in. (10.16 cm) radius.

Again comparing the two circular profiles it could be concluded that using a smaller radius would require a larger depth, a higher pressure or a change in channel geometry in order to obtain an effective area comparable to the larger radius design. For a given application, the depth may be limited by space constraints. The maximum pressure is directly linked to the maximum vapor temperature which will be limited by the maximum allowable temperature of the source. Altering the channel geometry to increase opening sensitivity will result in higher material stresses limiting the choices of envelope material. In addition to increasing the width  $2R$  and the depth  $Z$ , the height of the radiator can be increased, within space constraints, by forming the tear-drop shape. As can be seen in Figure 10, extending the height of the radiator can result in a significant increase in the effective area. This was primarily due to the increase in physical surface area rather than a change in view factor.

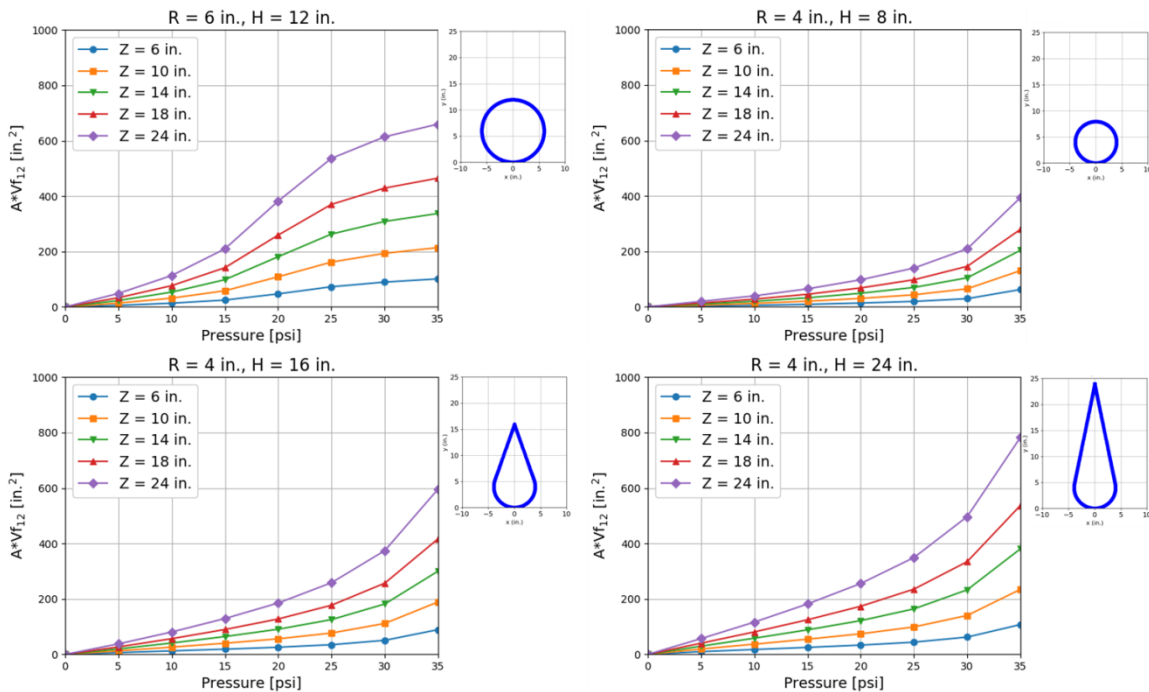


**Figure 10. Effective Area ( $AV_{f,12}$ ) of the four profiles as functions of internal pressure and radiator depth  $Z$ . Wall thickness = 0.025 in., channel width = 2.0 in. and vapor space gap = 0.02 in.**

### C. Demonstration of Temperature Control Capability

During a design process it is necessary to size the radiator to be capable of dissipating the maximum input power  $Q_{max}$  at the maximum sink temperature  $T_{s,max}$ . To size a VVFTPR it is necessary to select the depth  $Z$  and a profile, controlled by  $R$  and  $H$ , that result in an effective area  $AV_{f,12}$  capable of dissipating  $Q_{max}$  at the maximum sink temperature. The VVFTPR has the additional constraint that the vapor temperature must not exceed the maximum allowable vapor temperature  $T_{v,max}$ , which will be dictated by the maximum temperature of the electronics.

In order to utilize the thermal model described in Section III. it was necessary to select several values to be used in the calculation. For this section, the maximum power input was  $Q_{max} = 40$  W and the sink temperature was varied

between  $-130^{\circ}\text{C}$  and  $20^{\circ}\text{C}$ . The emissivity was set to 0.92. The maximum allowable vapor temperature  $T_{v,max}$  was selected to be  $60^{\circ}\text{C}$ .

It was also necessary to specify the working fluid because of the relationship between the vapor pressure and the vapor temperature. In order to utilize the results presented in Figure 10, a working fluid with vapor pressure below 35 psi (241.3 kPa) at the selected maximum vapor temperature of  $60^{\circ}\text{C}$  was required. For this section, pentane was selected as it has a vapor pressure of approximately 31 psi (213.7 kPa) at  $60^{\circ}\text{C}$ .

In order to size the VVFTPR to be capable of meeting these thermal requirements it was necessary to solve Eq. (2) and Eq. (3) for the effective area  $AV_{f,12}$  with inputs of  $Q_{max}$ ,  $T_{s,max}$  and  $T_{v,max}$ . Note that to solve for this product the thermal resistances due to conduction and condensation must be neglected. At the low temperatures discussed here the thermal resistance due to radiation will be several orders of magnitude higher than the other sources of resistance justifying dropping these terms from Eq. (3). For the thermal conditions described above it was determined that an effective area of approximately  $234\text{ in.}^2$  ( $0.151\text{ m}^2$ ) at  $T_{v,max}$  was required. For a given profile shape, the necessary value of  $Z$  could then be determined by interpolating within the data shown above in Figure 10. Table 2 lists the depth  $Z$  necessary to meet the thermal requirements for the four profiles. Note that these values are rounded to the nearest multiple of the channel width of 2.0 in. (5.08 cm) Table 2 also lists the actual physical surface area of the radiators. Because the radiators were all sized for the same conditions a smaller surface area implies a higher view factor at  $T_{v,max}$ .

**Table 2. Radius, height, depth and the corresponding actual surface area of the four VVFTPR profiles.  $Z$  selected to obtain the required effective area to dissipate 40W at a sink temperature of  $20^{\circ}\text{C}$  and vapor temperature of  $60^{\circ}\text{C}$ .**

$R$ (in.)	$H$ (in.)	$Z$ (in.)	Actual Surface Area (in. <sup>2</sup> )
6.0	12.0	12.0	452.4
4.0	8.0	24.0	603.2
4.0	16.0	16.0	606.1
4.0	24.0	14.0	748.9

Figure 11 shows the variation in vapor temperature with sink temperature for the four VVFTPRs listed in Table 2. Figure 11 also shows the performance of a “Standard Radiator” which represents a flat ( $V_{f,12} = 1$ ) isothermal surface sized to dissipate  $Q_{max}$  at  $T_{s,max}$ . The “Standard Radiator” has no means of temperature control and the thermal model showed this radiator would experience a vapor temperature swing of approximately  $63^{\circ}\text{C}$  over the given sink temperature range. The VVFTPRs on the other hand exhibited excellent thermal control for the same power and sink conditions. Table 3 lists the maximum change in vapor temperature observed in Figure 11 for the four profiles. The smallest temperature change of  $11.4^{\circ}\text{C}$  occurred for the 4.0 in. (10.16 cm) circular profile while the largest temperature change of  $15.9^{\circ}\text{C}$  occurred for the 6.0 in. (15.24 cm) circular profile.

**Table 3. Maximum change in vapor temperature of the four profiles for a sink temperature range of  $-130^{\circ}\text{C}$  to  $20^{\circ}\text{C}$ .**

$R$ (in.)	$H$ (in.)	$T_{v,max} - T_{v,min}$
6.0	12.0	15.9
4.0	8.0	11.4
4.0	16.0	12.8
4.0	24.0	14.2

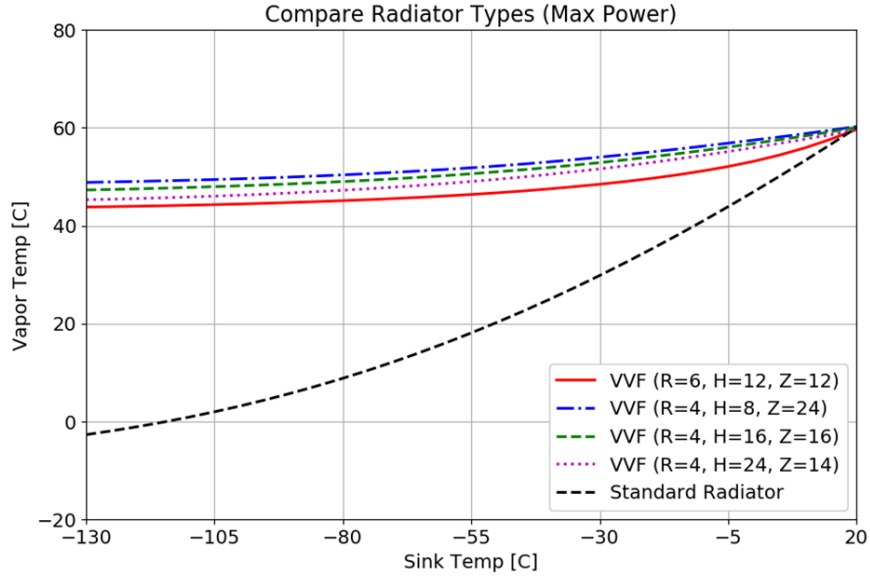


**Figure 11. Variation in vapor temperature with sink temperature for the radiator geometries listed in Table 1. A “Standard Radiator” represents a flat radiator ( $V_{f,12} = 1$ ) sized to dissipate max power at max sink temperature. Max Power = 40 W.**

The temperature control of the VVFTPR is driven by the rate of change of view factor  $V_{f,12}$  with vapor pressure. Figure 12 shows the variation of  $V_{f,12}$  with pressure for the four profiles discussed above. Recall that for pentane as the working fluid the pressure at  $T_{v,max}$  was approximately 31 psi (213.7 kPa). It can be seen that the 6.0 in. (15.24 cm) circular profile had the largest view factor at 31 psi (213.7 kPa) and therefore required the smallest area as shown in Table 2; however, the same profile exhibited decreased opening sensitivity at higher pressures. For a given drop in sink temperature a larger drop in vapor temperature was therefore required to balance the system. While the four profiles exhibited different levels of temperature control, these differences were relatively small compared to a radiator with no temperature control. As a result the best choice would likely be the profile that obtains the highest view factor at  $T_{v,max}$  while fitting within any space constraints. This profile would have the smallest physical surface area and therefore the lowest mass. Of the four profiles investigated above, the circular profile with  $R = 6$  in. (15.24 cm),  $H = 12.0$  in. (30.48 cm) and  $Z = 12.0$  in. (30.48 cm) has the smallest surface area and therefore the lowest mass.

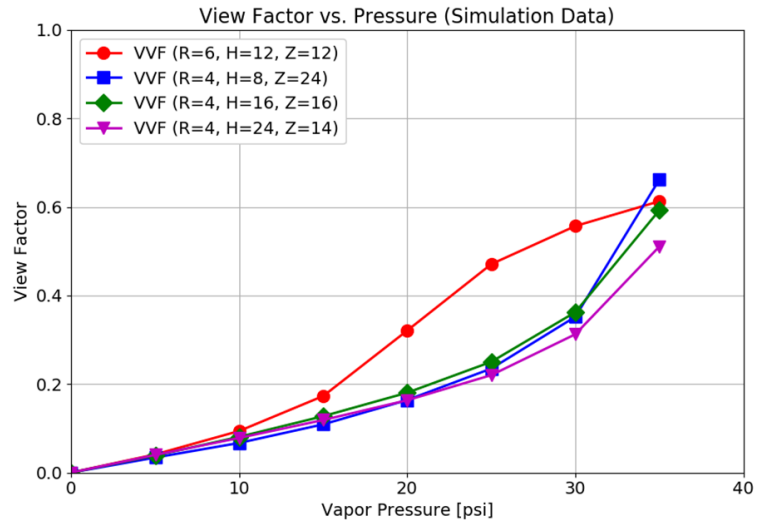


**Figure 12. Variation in view factor  $V_{f,12}$  with vapor pressure for the 4 profiles listed in Table 1.**

A key feature of the VVFTPR is the ability to maintain the temperature within the operating range of the electronics despite wide variations in heat sink temperature and heat loads. At a given point during a mission the electronics may be operating at a reduced load during a time when the sink temperature is minimum. For the results presented in this section, if it is assumed that the electronics have a minimum operating temperature of  $-30^{\circ}\text{C}$  then at the minimum sink temperature of  $-130^{\circ}\text{C}$  the flat panel radiator would require a minimum of 25W to maintain the electronics above the minimum operating temperature of  $-30^{\circ}\text{C}$ . Depending on the operating schedule of the electronics, significant heater

power may be required to maintain the vapor at a sufficiently high temperature. The VVFTPR on the other hand requires only 0.33W of power to maintain the vapor above  $-30^{\circ}\text{C}$  at the minimum sink temperature of  $-130^{\circ}\text{C}$ , a reduction in required power by a factor of 75. This power would likely easily be supplied by the electronics operating at a reduced load and therefore little to no heater power would be required.

## V. Conclusion

In previous work,<sup>4</sup> ACT demonstrated an innovative variable-view-factor two-phase radiator prototype. The VVFTPR utilizes two-phase heat transfer to both spread the heat resulting in high radiating efficiency and to control the view factor of the radiating surface. The concept allows for passive thermal control of the source temperature as the heat load and heat sink conditions change. This paper extended the previous structural modeling to three dimensions and introduced a thermal model of the VVFTPR. Three-dimensional structural simulations were used to parametrically investigate the effects of channel width, vapor space gap and wall thickness on the view factor. Design tradeoffs involved in changing each variable were discussed. The structural simulations were then used to investigate the effect of the profile shape on the effective area presented by the VVFTPR, and a process for using the simulation data to size a VVFTPR for a given thermal environment was discussed. Finally, the thermal model was used to demonstrate the temperature control feature of the VVFTPR. For the given thermal conditions it was demonstrated that the VVFTPR was able to reduce the temperature drop by a factor of 4 to 6 relative to a flat panel radiator with no temperature control while operating at maximum power. It was also demonstrated that the VVFTPR is capable of maintaining electronics above minimum operating temperatures even at very low heat loads and heat sink temperatures without the use of heater power.

It is important to note that because the maximum view factor obtained by the VVFTPR is less than 1.0, the VVFTPR is necessarily larger and heavier than a flat panel radiator sized to reject an equivalent load. Despite this the VVFTPR has several advantages.

- The thermal control capability of the VVFTPR will require little to no heater power during low power operation in order to maintain electronics above the minimum operating limit.
- During survival mode the VVFTPR will be fully closed resulting in significant thermal resistance and therefore a significant reduction in heat power required for survival.
- Due to its shape changing capability the VVFTPR is automatically deployable. In the fully closed position for launch it will have a smaller foot print than an equivalent flat panel radiator.

Future work on this concept will include:

- Further 3D structural simulations in order to optimize the design.
- An investigation to determine the ideal envelope material and manufacturing method.
- Experimental work to verify the results of the model.

## Acknowledgments

This project is funded by NASA Marshall Space Flight Center under a SBIR Phase II program (Contract 80NSSC18P2187). The technical monitor is Jeff Farmer.

## References

- <sup>1</sup> Viswanatha, N. and Murali, T., "A Novel Mechanism using Shape Memory Alloy to Drive Solar Flaps of the INSAT-2E Satellite," Proceedings of the 34th Aerospace Mechanisms Symposium, pp. 241–251, 2000.
- <sup>2</sup> Christopher L. Bertagne, Rubik B. Sheth, Darren J. Hartl, and John D. Whitcomb, "Simulating Coupled Thermal-Mechanical Interactions in Morphing Radiators," Proceedings of the SPIE, Volume 9431, 94312F, 2015.
- <sup>3</sup> NASA Technology Roadmaps, TA 14: Thermal Management Systems, July 2015.
- <sup>4</sup> Lutz, A., Tarau, C. and Rokkam, S., "Variable-View-Factor Two-Phase Radiator", ICES-2019-211, 49<sup>th</sup> International Conference on Environmental Systems, 2019.
- <sup>5</sup> Rokkam, S., Tarau, C. and Lutz, A., "Variable-View-Factor Two-Phase Radiator," NASA SBIR Phase I Final Report, Contract NO. 80NSSC18P2187, 2019